Applied Catalysis B: Environmental 138–139 (2013) 299–303

Contents lists available at SciVerse ScienceDirect

Applied Catalysis B: Environmental

journal homepage: www.elsevier.com/locate/apcatb

Hierarchical porous CdS nanosheet-assembled flowers with enhanced visible-light photocatalytic H_2-production performance

Quanjun Xiang[a,b], Bei Cheng[b], Jiaguo Yu[b,*]

[a] Key Laboratory of Arable Land Conservation (Middle and Lower Reaches of Yangtse River), Ministry of Agriculture, College of Resources and Environment, Huazhong Agricultural University, Wuhan 430070, PR China

[b] State Key Laboratory of Advanced Technology for Material Synthesis and Processing, Wuhan University of Technology, Luoshi Road 122#, Wuhan 430070, PR China

ARTICLE INFO

Article history:
Received 4 January 2013
Received in revised form 16 February 2013
Accepted 1 March 2013
Available online 14 March 2013

Keywords:
Hierarchical
Porous CdS nanosheet
Ion-exchange strategy
Photocatalytic H_2-production activity

ABSTRACT

Hierarchical porous CdS nanosheet-assembled flowers were synthesized by a simple ion-exchange strategy using morphology-analogous $Cd(OH)_2$ and Na_2S as precursors. The prepared CdS flowers exhibited high visible-light photocatalytic H_2-production activity with a rate of 468.7 $\mu mol\,h^{-1}$ and the corresponding apparent quantum efficiency (QE) of 24.7% at 420 nm, which exceeded that obtained on CdS nanoparticles by more than 3 times. This enhanced photocatalytic H_2-production activity was achieved because the hierarchical organization of nanosheets and porous nanosheet structures can efficiently enhance light-absorption ability and provide a greater number of active adsorption sites. This work shows a great potential of hierarchical porous CdS nanosheet-assembled flowers for photocatalytic H_2 production, and also demonstrates that the ion-exchange strategy of $Cd(OH)_2$ intermediates can be extended to the preparation of other porous oxides and sulfides with hierarchical nanostructures.

1. Introduction

The controlled synthesis of inorganic materials with desired morphologies and architectures at micro- and nanoscale levels is a key challenge in materials chemistry [1–3]. Fabrication of porous nanostructures has received considerable attention recently because of the potential applications of these materials for example in nanoreactors, catalysis, energy storage, solar cell, CO_2 capture, and controlled delivery [4–9]. Among materials with various shapes, nanosheets have attracted intensive interests as sheet-like materials with predominantly exposed crystal facets may exhibit improved catalytic performance over their wire-like or spherical structures due to their high surface-to-volume ratio [10–12]. However, the efficient synthesis of hierarchical porous sheet-like materials with high surface-to-volume ratio still remains a great experimental challenge.

As an important II–VI semiconductor with a direct band gap of 2.4 eV, CdS has attracted much research interest in recent years due to its excellent luminescent and photochemical properties [13–17]. CdS has been widely exploited for diverse applications such as photovoltaics, photoconductors, logic gates, light-emitting diodes, and dye-sensitized solar cells [16,17]. In addition, CdS has been demonstrated to be an excellent photocatalytic material for the production of hydrogen from water splitting under visible-light irradiation [13–15]. Considering its wide applications, various CdS nanostructures have been prepared during the past few years. For example, Jun et al. reported the controlled synthesis of multi-armed CdS nanorod architectures using mono-surfactant system [18]. Barrelet et al. reported the preparation of CdS nanowires using single-source molecular precursor by a gold nanocluster-catalyzed vapor–liquid–solid growth mechanism [19]. However, hierarchical porous CdS nanosheet-assembled flowers and their photocatalytic H_2-production activity were seldom reported in the previous studies.

In this paper, hierarchical flower-like CdS nanostructure assembled from porous nanosheets are prepared by a simple anion exchange using hydrothermally synthesized $Cd(OH)_2$ nanosheet-assembled flowers and Na_2S as precursors. The as-prepared porous CdS nanosheet-based flower-like assemblies are highly active for photocatalytic H_2 evolution from water splitting under visible-light. In addition, the ion-exchange strategy of $Cd(OH)_2$ intermediates is also suitable for fabricating other porous oxide and sulfide nanostructures. To the best of our knowledge, this is the first report on the preparation and photocatalytic H_2-production activity of hierarchical porous CdS nanosheet-assembled flowers by the ion-exchange strategy.

* Corresponding author.
E-mail address: jiaguoyu@yahoo.com (J. Yu).

0926-3373/$ – see front matter © 2013 Elsevier B.V. All rights reserved.
http://dx.doi.org/10.1016/j.apcatb.2013.03.005

2. Experimental details

2.1. Synthesis of $Cd(OH)_2$ nanosheets-based assemblies

All chemicals used in this study were analytical grade (purchased from Shanghai Chemical Industrial Company) and were used without further purification. Deionized water was used in all experiments. The $Cd(OH)_2$ assemblies were synthesized by a hydrothermal method. In a typical synthesis, 1 mmol of $CdCl_2{\cdot}2H_2O$ was dissolved in 20 mL of distilled water, and then 30 mL of triethanolamine (TEA) was added dropwise into the above solution under magnetic stirring. After that, 20 mL of 2 M NaOH solution was added under stirring. The mixed solution was then transferred into a dried 100 mL Teflon-lined autoclave and maintained for 12 h at 120 °C. After the reaction, the autoclave was allowed to cool to room temperature, and the white precipitate was collected by centrifugation, washed three times with distilled water and ethanol, and then dried in an oven at 60 °C for 12 h.

2.2. Synthesis of hierarchical porous CdS nanosheet-assembled flowers

Hierarchical porous CdS nanosheet-assembled flowers were synthesized by a simple anion-exchange strategy. The as-prepared $Cd(OH)_2$ nanosheets-based assemblies were used as precursors. In a typical synthesis, 0.3 g of as-prepared $Cd(OH)_2$ powder was dispersed in 50 mL of distilled water under magnetic stirring. Then, 25 mL of 0.1 M $Na_2S{\cdot}9H_2O$ was added into the above solution under continuous stirring for 1 h. After that, the red precipitate was collected by centrifugation, washed three times with distilled water and ethanol, and then dried in an oven at 60 °C for 12 h. For the purpose of comparison, the CdS nanoparticles were also prepared according to the procedure reported elsewhere [15].

2.3. Characterization

XRD patterns were obtained on a D/Max-RB X-ray diffractometer (Rigaku, Japan) using Cu Kα radiation at a scan rate of 0.05° $2\theta\,s^{-1}$. The accelerating voltage and the applied current were 40 kV and 80 mA, respectively. Scanning electron microscopy (SEM) was performed using a S-4800 microscope (Hitachi, Japan). Transmission electron microscopy (TEM) analyses were conducted with a JEM-2100F electron microscope (JEOL, Japan), using a 200 kV accelerating voltage. The Brunauer–Emmett–Teller specific surface areas (S_{BET}) and porosity of the samples were evaluated on the basis of nitrogen adsorption isotherms measured at −196 °C using a Micromeritics ASAP 2020 gas adsorption apparatus (USA). All the samples were degassed at 180 °C before nitrogen adsorption measurements. The BET surface area was determined using adsorption data in the relative pressure (P/P_0) range of 0.05–0.3. A desorption isotherm was used to determine the pore size distribution via the Barrett–Joyner–Halenda (BJH) method, assuming a cylindrical pore model [20]. The nitrogen adsorption volume at the relative pressure (P/P_0) of 0.99 was used to determine the single-point pore volume and the average pore size. UV–visible absorbance spectra were obtained for the dry-pressed disk samples by a UV–visible spectrophotometer (UV-2550, Shimadzu, Japan). $BaSO_4$ was used as a reflectance standard in a UV–visible diffuse reflectance experiments.

2.4. Evaluation of photocatalytic activity

The photocatalytic H_2-production experiments were performed in a 100 mL Pyrex flask at ambient temperature and atmospheric pressure, and three openings of the flask were sealed with silicone rubber septum. A 350 W Xe arc lamp through a UV-cutoff filter (≦420 nm) positioned 5 cm in front of the photocatalytic reactor was used as a visible-light source (22 cm far away from the photocatalytic reactor). The focused light intensity on the flask measured using a visible-light radiometer (Model: FZ-A, China) was ca. 150 mW/cm^2 in the wavelength range of 420–1000 nm. In a typical photocatalytic experiment, 50 mg of the photocatalyst was suspended in 80 mL of a mixed solution of lactic acid (8 mL) and water (72 mL) under magnetic stirring and side-irradiation. A certain amount of $H_2PtCl_6{\cdot}6H_2O$ aqueous solution was dripped into the system to load 0.5 wt% Pt onto the surface of the photocatalyst by a photochemical reduction deposition method. Prior to irradiation, the system was bubbled with nitrogen for 30 min to remove the dissolved oxygen. A continuous magnetic stirrer was applied at the bottom of the reactor in order to keep the photocatalyst particles in suspension status during the whole experiment. A 0.4 mL of gas was sampled intermittently through the septum, and hydrogen was analyzed by gas chromatograph (GC-14C, Shimadzu, Japan, TCD, nitrogen as a carrier gas and 5 Å molecular sieve column). All glassware was carefully rinsed with deionized water prior to use. The apparent quantum efficiency (QE) was measured under the same photocatalytic reaction conditions. Four low power UV-LEDs (3 W, 420 nm, Shenzhen LAMPLIC Science Co. Ltd., China), which were positioned 1 cm away from the reactor in four different directions, were used as light sources to trigger the photocatalytic reaction. The focused intensity and areas on the flask for each UV-LED was ca. 6.0 mW/cm^2 and 1 cm^2, respectively. The QE was calculated according to the following equation:

$$\begin{aligned}\mathrm{QE}\ [\%] &= \frac{\text{number of reacted electrons}}{\text{number of incident photons}} \times 100 \\ &= \frac{\text{number of evolved } H_2 \text{ molecules} \times 2}{\text{number of incident photons}} \times 100 \end{aligned} \qquad (1)$$

3. Results and discussion

Hierarchical porous CdS nanosheet-assembled flowers were prepared by a simple ion-exchange strategy using hydrothermally synthesized $Cd(OH)_2$ and Na_2S as precursors. As shown in Fig. 1a, the $Cd(OH)_2$ nanosheet-assembled flowers are first prepared using a modified amine-assisted hydrothermal method, and then react with S^{2-} anions to obtain nanoporous CdS nanosheet-assembled flowers. Typical XRD patterns of the as-prepared intermediate precursors identify them as the hexagonal $Cd(OH)_2$ (JCPDS no. 31-0228) (see Fig. 1b). After the $Cd(OH)_2$ precursors react with S^{2-} anions, the red products are obtained immediately and these products are assigned to the hexagonal phase of CdS (JCPDS no. 41-1049) by the XRD patterns (Fig. 1b). UV–visible diffuse absorption spectra (see Fig. 1c) also confirm that the white powder precursors with the bandgap energy of 3.9 eV can be successfully transformed into red CdS products with the intrinsic bandgap of 2.2 eV. The above direct band gaps of the powder samples are determined according to the Kubelka–Munk method [21–24]. This structure transformation induced by ion exchange is because the solubility product (K_{sp}) of CdS (8.0×10^{-27}) is much smaller than that of $Cd(OH)_2$ (2.5×10^{-14}), and thus $Cd(OH)_2$ can be spontaneously transformed into CdS in the presence of S^{2-}. These results imply that the ion exchange reactions of the $Cd(OH)_2$ materials with sulfur anions can lead to the formation of hexagonal CdS.

Fig. 2a shows a typical SEM image of the hydrothermal-synthesized $Cd(OH)_2$ precursor before exchange. The $Cd(OH)_2$ products are novel flower-like hierarchical assemblies with an average particle size of approximately 5 μm. As shown in Fig. 2b, the flower-like $Cd(OH)_2$ assemblies are further constructed from two-dimensional nanosheets having a thickness of several tens of nanometers and widths and lengths in the range of 500–800 nm.

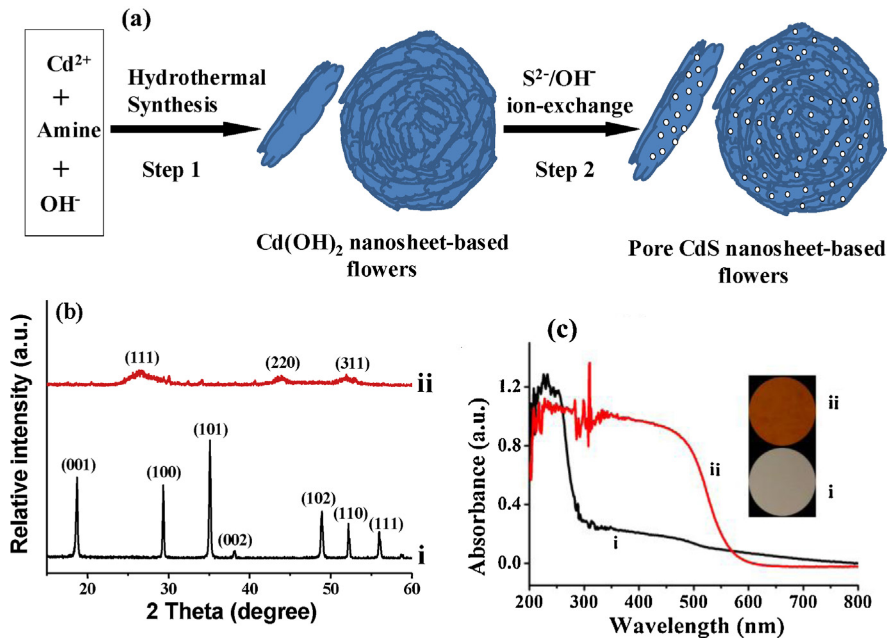

Fig. 1. (a) A schematic illustration of the synthesis route of porous CdS nanosheet-assembled flowers. (b) XRD patterns and (c) UV–visible diffuse absorption spectra and the corresponding photos (insets) of (i) the $Cd(OH)_2$ intermediates and (ii) the as-prepared CdS products.

These nanosheets interconnect with each other to form a 3D structure having pores of different sizes, which can serve as transport paths for small molecules [25,26]. It is noteworthy that the ion-exchange reaction has little influence on the overall morphology of the final products. In principle, each $Cd(OH)_2$ nanosheet functions as a self-template for forming the resultant CdS nanosheets during the ion-exchange reaction. The structure of the nanosheets and their hierarchical assemblies are basically retained after the subsequent ion exchange (see Fig. 2c and d).

Fig. 3a and b shows the TEM images of $Cd(OH)_2$ and CdS nanosheets, respectively. Obviously, the $Cd(OH)_2$ solid sheets become nanoporous CdS nanosheets with a pore size of 5–10 nm. In this case, how does this porous structure within the nanosheets form? It is proposed that most of the hydroxyl ions in $Cd(OH)_2$ nanosheets have been exchanged with sulfur anions in a very short time due to the great difference of solubility products of CdS and $Cd(OH)_2$, indicating the rapid kinetics of this ion-exchange reactions. The rapid kinetics and stain release can result in the

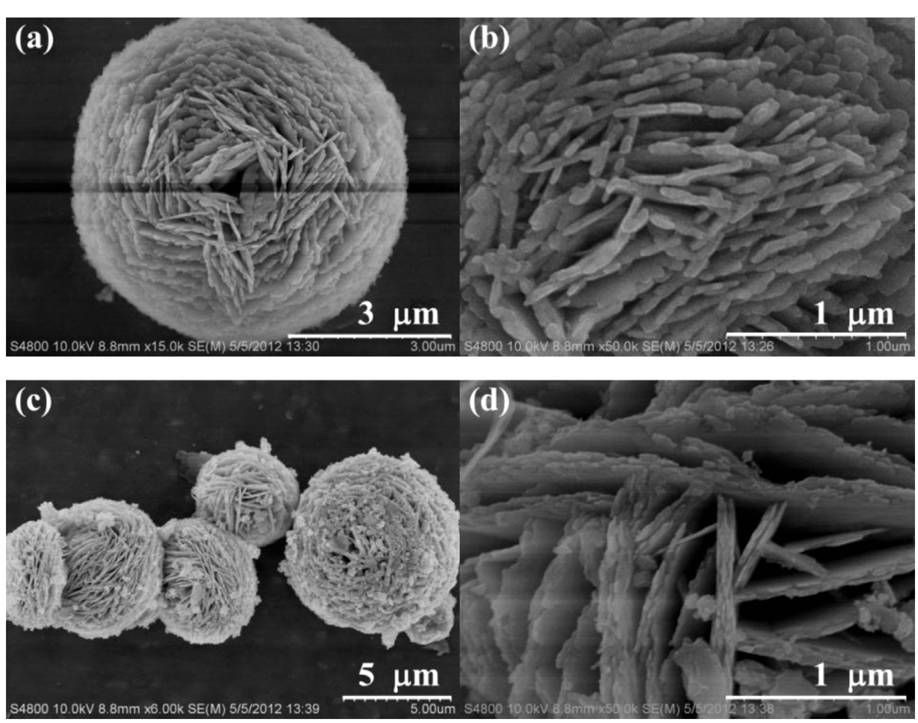

Fig. 2. (a, c) Low- and (b, d) high-magnification SEM images of the $Cd(OH)_2$ intermediates (a, b) and the as-prepared CdS products (c, d).

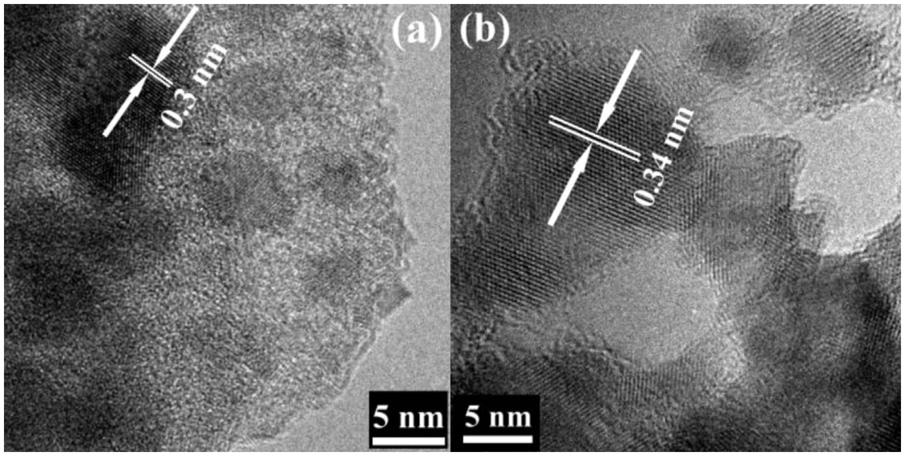

Fig. 3. TEM images of the $Cd(OH)_2$ intermediates (a) and the as-prepared CdS products (b).

appearance of voids and/or pores because of large lattice mismatch (13%) between CdS and $Cd(OH)_2$. In addition, the density of CdS (4.65 g/cm^3) is smaller than that of $Cd(OH)_2$ (4.79 g/cm^3), and the volume expansion is also responsible for the appearance of pores. The present results are similar to the previous studies showing that the partial cation exchange can promote the strain-driven formation of pore and hollow structures [27–31]. In addition, the TEM images (Fig. 3a and b) of $Cd(OH)_2$ and CdS nanosheets show many random arranged domains with short-range continuous crystal lattices, indicating a polycrystalline nature of the $Cd(OH)_2$ and CdS nanosheets. The lattice fringes of individual nanoparticle with d spacing of ca. 0.3 and 0.34 nm can be assigned to the (1 0 0) and (0 0 2) planes of hexagonal Cd(OH) and CdS, respectively.

The porous structures and textures of the CdS flowers observed by SEM and TEM were further elucidated by nitrogen sorption analysis. Fig. 4 shows nitrogen sorption isotherms and the corresponding pore size distribution curve for the CdS nanostructure. The isotherms are of type IV with a narrow hysteresis loop at high relative pressures, characteristic of mesopores (mesopores have widths between 2 and 50 nm) and macropores (>50 nm) features [20,32,33]. The shapes of the hysteresis loops are of type H3, suggesting narrow slit-shaped pores that are generally associated with sheet-like particles [20,32,33]. This also agrees well with their morphology (see Figs. 2c, d and 3b) with the mesopores arising from the voids within CdS nanosheets and the interspaces between their hierarchical organizations. Such a porous structure is further confirmed by the corresponding pore size distributions (inset in Fig. 4). The BET specific surface area of the CdS flowers is 57.8 m^2/g, indicating that the sample has a relatively high surface-to-volume ratio for crystalline metal sulfide.

To demonstrate the potential applicability of the hierarchical porous CdS nanosheet-assembled flowers in photocatalytic H_2 production and the effects of morphology on the photocatalytic activity, we examined its photocatalytic H_2-production activity in relation to that of the prepared CdS nanoparticles with sizes from ca. 20 to 50 nm (see Fig. 5) under visible light using lactic acid as scavenger and Pt as co-catalyst. Fig. 6 shows the reaction time courses of photocatalytic H_2 production over porous CdS nanosheets and CdS nanoparticles. As seen in Fig. 6, the photocatalytic reaction for porous CdS nanosheets shows a steady H_2 generation, and the H_2 production rate reaches the value of 468.7 μmol h^{-1} with an apparent quantum efficiency (QE) of 24.7% at 420 nm, which exceeded that obtained on CdS nanoparticles (with a QE of 8.2%) by more than 3 times. This high H_2-production photoactivity can be ascribed to the hierarchical porous nanosheet-assembled structures. The space of inter-meshed nanosheets is beneficial to multiple reflections of trapped incident light, thus enhancing light harvesting and increasing the quantities of photogenerated electrons and holes that participate in photocatalytic reactions [25,26,34,35]. Furthermore, in comparison with other

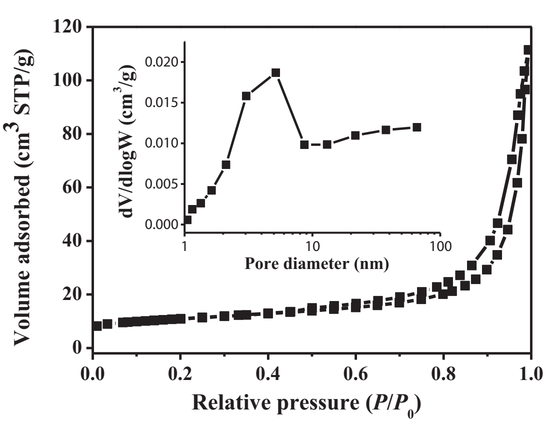

Fig. 4. Nitrogen adsorption–desorption isotherm and the corresponding pore size distribution (inset) of porous CdS nanosheet-assembled flowers.

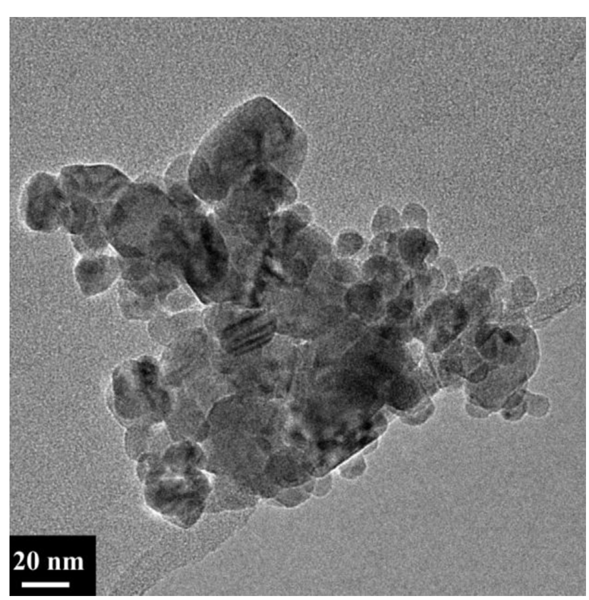

Fig. 5. TEM image of the as-prepared CdS nanoparticles.

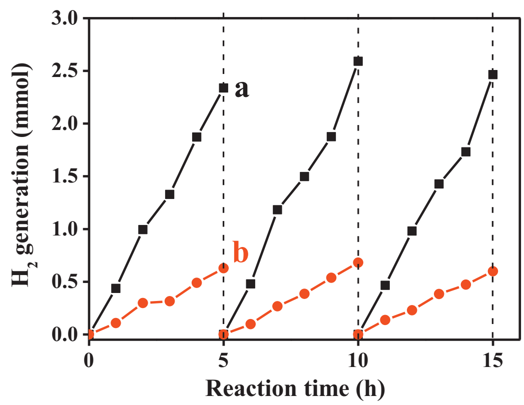

Fig. 6. Time course of photocatalytic production of H_2 from lactic acid aqueous solutions over (a) the porous CdS nanosheet-assembled flowers and (b) CdS nanoparticles under visible-light irradiation.

solid nanostructures, the porous structure possess higher surface-to-volume ratio, which assures the higher total amount of the surface active sites available for adsorption of reactant molecules and facilitates the mass transfer, hence enhancing the photocatalytic efficiency [35–43].

4. Conclusions

In summary, we report the synthesis of porous CdS nanosheet-based flower-like assemblies by ion-exchange reactions of the hydrothermally synthesized $Cd(OH)_2$ nanosheet-assembled flowers with S^{2-} anions. The prepared porous CdS nanosheet-assembled flowers showed high visible-light photocatalytic H_2 production activity with a rate of 468.7 μmol h^{-1} and the corresponding apparent QE of 24.7% at 420 nm. It is believed that the hierarchical porous organization of nanosheets can efficiently enhance light-absorption ability and provide a greater number of active adsorption sites, and consequently improve the photocatalytic H_2 production activity. This work shows a great potential of hierarchical porous CdS nanosheet-assembled flowers for photocatalytic H_2 production, and also demonstrates that the ion-exchange strategy of $Cd(OH)_2$ intermediates can be extended to the preparation of other porous oxides and sulfides with hierarchical nanostructures.

Acknowledgements

This work was partially supported by the 973 program (2013CB632402), 863 program (2012AA062701), NSFC (51072154, 21177100 and 51272199), Fundamental Research Funds for the Central Universities and Self-determined and Innovative Research Funds of SKLWUT.

References

[1] H. Colfen, S. Mann, Angewandte Chemie International Edition 42 (2003) 2350.
[2] S.W. Liu, J.G. Yu, M. Jaroniec, Journal of the American Chemical Society 132 (2010) 11914.
[3] Q.J. Xiang, J.G. Yu, M. Jaroniec, Chemical Communications 47 (2011) 4532.
[4] J. Liu, S.Z. Qiao, S.B. Hartono, G.Q. Lu, Angewandte Chemie International Edition 49 (2010) 4981.
[5] J.H. Park, S. Kim, A.J. Bard, Nano Letters 6 (2006) 24.
[6] M. Ksibi, S. Rossignol, J.M. Tatibouet, C. Trapalis, Materials Letters 62 (2008) 4204.
[7] G.T. Li, H.Y. Yip, C. Hu, P.K. Wong, Materials Research Bulletin 46 (2011) 153.
[8] K.P. Gierszal, M. Jaroniec, Chemical Communications (2004) 2576.
[9] J.G. Yu, Y. Le, B. Cheng, RSC Advances 2 (2012) 6784.
[10] H.G. Yang, C.H. Sun, S.Z. Qiao, J. Zou, G. Liu, S.C. Smith, H.M. Cheng, G.Q. Lu, Nature 453 (2008) 638.
[11] J. Zhang, J.G. Yu, Y. Zhang, Q. Li, J.R. Gong, Nano Letters 11 (2011) 4774.
[12] Q.J. Xiang, J.G. Yu, M. Jaroniec, Nanoscale 3 (2011) 3670.
[13] Q.J. Xiang, J.G. Yu, M. Jaroniec, Chemical Society Reviews 41 (2012) 782.
[14] Q. Li, B. Guo, J.G. Yu, J.R. Ran, B. Zhang, H. Yan, J.R. Gong, Journal of the American Chemical Society 133 (2011) 10878.
[15] J.R. Ran, J.G. Yu, M. Jaroniec, Green Chemistry 13 (2011) 2708.
[16] T. Ni, D.K. Nagesha, J. Robles, N.F. Materer, S. Mussig, N.A. Kotov, Journal of the American Chemical Society 124 (2002) 3980.
[17] A. Kudo, Y. Miseki, Chemical Society Reviews 38 (2009) 253.
[18] Y.W. Jun, S.M. Lee, N.J. Kang, J. Cheon, Journal of the American Chemical Society 123 (2001) 5150.
[19] C.J. Barrelet, Y. Wu, D.C. Bell, C.M. Lieber, Journal of the American Chemical Society 125 (2003) 11498.
[20] K.S.W. Sing, D.H. Everett, R.A.W. Haul, L. Moscou, R.A. Pierotti, J. Rouquerol, T. Siemieniewska, Pure and Applied Chemistry 57 (1985) 603.
[21] P.J. Kubelka, Optical Society of America 38 (1948) 448.
[22] J.G. Yu, X.X. Yu, Environmental Science and Technology 42 (2008) 4902.
[23] J. Zhang, J.G. Yu, M. Jaroniec, J.R. Gong, Nano Letters 12 (2012) 4584.
[24] Y.S. Li, F.L. Jiang, Q. Xiao, R. Li, K. Li, M.F. Zhang, A.Q. Zhang, S.F. Sun, Y. Liu, Applied Catalysis B 101 (2010) 118.
[25] S.W. Liu, C. Li, J.G. Yu, Q.J. Xiang, CrystEngComm 13 (2011) 2533.
[26] X.X. Yu, J.G. Yu, B. Cheng, M. Jaroniec, Journal of Physical Chemistry C 113 (2009) 17527.
[27] S.E. Wark, C.H. Hsia, D.H. Son, Journal of the American Chemical Society 130 (2008) 9550.
[28] A. Cabot, R.K. Smith, Y.D. Yin, H.M. Zheng, B.M. Reinhard, H.T. Liu, A.P. Alivisatos, ACS Nano 2 (2008) 1452.
[29] N. Bao, L. Shen, T. Takata, K. Domen, Chemistry of Materials 20 (2008) 110.
[30] Y. Yu, J. Zhang, X. Wu, W. Zhao, B. Zhang, Angewandte Chemie International Edition 51 (2012) 897.
[31] V.P. Zhdanov, B. Kasemo, Nano Letters 9 (2009) 2172.
[32] M. Kruk, M. Jaroniec, Chemistry of Materials 13 (2001) 3169.
[33] Q.J. Xiang, J.G. Yu, M. Jaroniec, Journal of the American Chemical Society 134 (2012) 6575.
[34] P. Jiang, J.J. Zhou, H.F. Fang, C.Y. Wang, Z.L. Wang, S.S. Xie, Advanced Functional Materials 17 (2007) 1303.
[35] Q.J. Xiang, J.G. Yu, W.G. Wang, M. Jaroniec, Chemical Communications 47 (2011) 6906.
[36] J.G. Yu, J.C. Yu, M.K.P. Leung, W.K. Ho, B. Cheng, X.J. Zhao, J.C. Zhao, Journal of Catalysis 217 (2003) 69.
[37] Q.J. Xiang, K.L. Lv, J.G. Yu, Applied Catalysis B 96 (2010) 557.
[38] J.G. Yu, W.G. Wang, B. Cheng, Chemistry – An Asian Journal 5 (2010) 2499.
[39] W. Wang, J. Yu, Q. Xiang, B. Cheng, Applied Catalysis B 119–120 (2012) 109.
[40] P. Madhusudan, J. Ran, J. Zhang, J. Yu, G. Liu, Applied Catalysis B 110 (2011) 286.
[41] P. Madhusudan, J. Yu, W. Wang, B. Cheng, G. Liu, Dalton Transactions 41 (2012) 14345.
[42] J. Yu, Y. Yu, B. Cheng, RSC Advances 2 (2012) 11829.
[43] Q. Xiang, J. Yu, Chinese Journal of Catalysis 32 (2011) 525.